

Chapter 1

Developments in confocal virtual slit-scanning microscopy

— Rick Ricketts

Conventional epi-illumination fluorescence microscopes illuminate the focal plane of the detection objective as well as a large fraction of the sample outside the focal plane. This leads to background intensity due to out-of-focus fluorescence, affecting resolution and contrast. Confocal-microscopes use a pin-hole in a conjugate image plane to forcibly reject fluorescence from outside of the focal plane, producing overall better axially resolved images and contrast and resolution. Sectioning by this means, leads to a large photon dose throughout the sample and with a cost to overall speed. Light-sheet microscopes address this generally by illuminating with a *thin* sheet of light orthogonally to the sample; but for having wide-field contrast and optical sectioning being on the order of the thickness of the light-sheet.

In this chapter the use of a virtual slit will be employed directly on the detection camera in the light-sheet microscope presented in this thesis. Methods will be introduced to improve the speed of acquisition and simulations introduced for other microscope systems that may benefit from confocal slit-scanning.

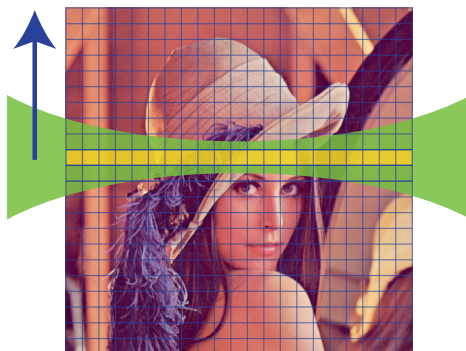


Fig. 1.1 The principle of confocal slit-scanning using digital light-sheet microscopy. An incident beam (green) approaches orthogonally to the direction of the rolling shutter, the shutter consists of a width of active pixels (yellow). The inactive pixels correspond to out-of-focus light and are rejected from the final image.

1.1 Single beam confocal slit-scanning

It was shown that a confocal microscope may be run faster by using a narrow slit rather than a pin-hole, increases contrast and resolution in one direction[1]. The same principle can be applied to a Digitally scanned Light-sheet Microscopy (DSLM), provided the propagation of the beam is in the same direction as the slit. By scanning the slit and the beam concomitantly, an increase in resolution and contrast may be achieved in one direction [2]. Moreover, the out-of-focus light then being rejected, increases the overall axial resolution in one imaging axis.

There exist several approaches for the implementation of such a confocal system. One approach is to add a slit in a conjugate image plane and synchronously shift a physical spatial slit with the scanning illumination. The forces involved in accelerating a physical slit would be, however, large as the slit would be moving at ~ 10 kHz linearly. A more practical approach would involve de-scanning the entire image onto a static slit using galvanometric mirrors, optically. This does introduce more complexity to a system, but has the potential to increase the overall available FOV beyond just the field number of the detection objective [3]. This technique was exploited to great effect by Huisken *et. al.* where de-scanning was used to keep the emission photons of the beam along one row of pixels on a camera. The remaining pixel rows of the detector were filled with spectral information by placing a diffractive element in emission path.

By selectively activating pixels on an scientific Complementary Metal-Oxide-Semiconductor (sCMOS) detector for reading-off, out-of-focus light may be rejected

in a similar fashion to a physical slit. The rolling of the shutter with a concomitant sweeping of a beam of light allows for live confocal imaging, depicted in Fig. 1.1. The width of the slit adjusts the contrast and resolution of the final image. When the slit is of a similar width to the waist of the incident beam the Signal to Noise ratio (SNR) will be maximal.

1.1.1 Optimisation

A characterisation of the optimal slit width of the virtual slit was needed to provide the best imaging contrast. To measure this, 200 nm fluorescent beads were suspended in 1 % agarose VII gel at a concentration of 2.3×10^3 parts/ml. The agarose was mounted by pipetting warm on to a lightly scratched PDMS bar, which helped adherence. Entire volumes ($2048 \times 2048 \times 100 \mu\text{m}$) were imaged per each varying each slit width. Beads were then localised manually through a axially projected image (see Chapter ??).

Of the 31 beads that were localised a single candidate bead was chosen that was not part of an aggregate, sufficiently bright and unobscured. By analysing both the SNR and the contrast of each cropped window around the candidate bead, it was shown that the ideal slit width was $2.51 \pm 0.05 \mu\text{m}$ which is on the order of the width of the incident laser beam, $2.3 \pm 0.2 \mu\text{m}$ (Fig. 1.2). The SNR was computed by taking the ratio of its summed squared magnitude of to that of the noise at varying slit widths. The contrast was calculated by fitting a Two Dimensional (2D) Gaussian to each image, with varying slit width, and plotting the fitted amplitude A with an offset B , from the 2D Gaussian model:

$$Ae^{-\left(\frac{(x-x_0)^2-(y-y_0)^2}{2\sigma^2}\right)} - B \quad (1.1)$$

1.2 Double speed slit-scanning microscopy

The sensor used in the Orca Flash v4 (as well as other sCMOS cameras including the Pco.Edge and Andor Zyla) consists of two adjacent Fairchild sCMOS sensors. In global shutter mode the shutter propagates outward (middle to top and middle to bottom) from the centre of the sensor simultaneously. The fastest exposure possible

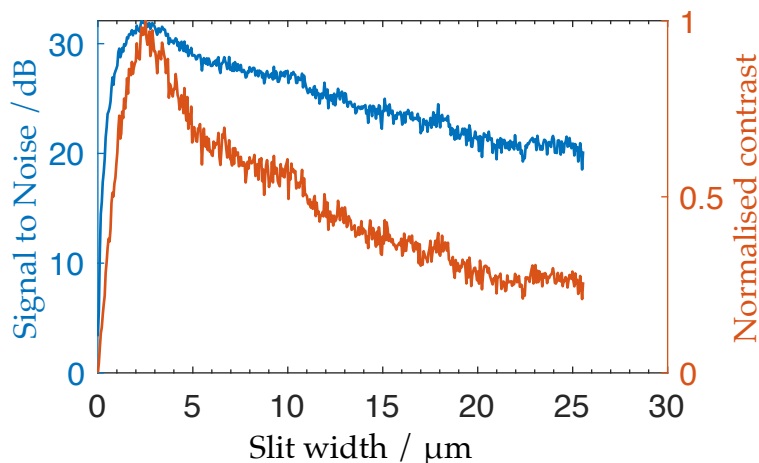


Fig. 1.2 Optimising the confocal slit width by varying slit width on a single fluorescent bead

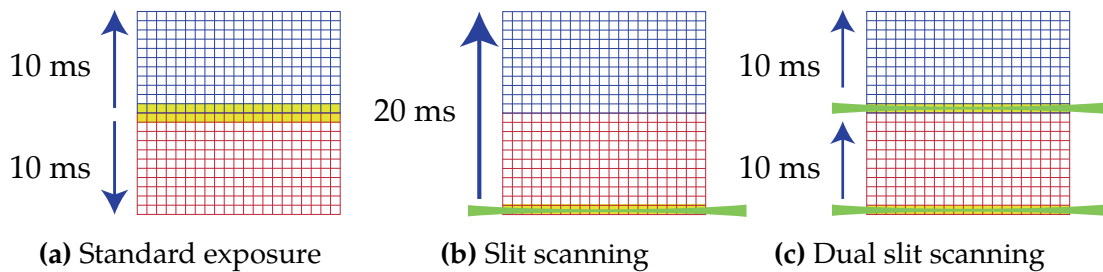


Fig. 1.3 The principle behind doubling the frame rate of the Orca Flash v4 when using slit-scanning mode. Standard exposure: In global shutter mode 100 Hz imaging may be achieved as each side of the sensor rolls an independent shutter. Slit-scanning: In normal slit-scanning mode the shutter moves from one half of the chip to the other serially, halving available frame-rate. Dual slit-scanning: The full frame-rate of the sensor is achievable when using two rolling shutters

for each chip (10ms) provides the maximum 100 Hz imaging for the full FOV. For confocal slit-scanning, the two sensors are addressed with a single thin shutter propagating from one side of one sensor (ex. bottom to middle) and across the next sensor (ex. middle to top), in series. In this mode the maximum frame rate achievable is 50 Hz as illustrated in Fig. 1.3.

In this work, a custom camera firmware was used to enable a pair of confocal slits, on each sensor half, to scan in the same direction simultaneously, providing the 100 Hz imaging that was ordinarily only available in global shutter mode.

1.2.1 Dual slits using an Spatial Light Modulator (SLM)

To exploit the new functionality of the two propagating shutters, two paraxial beams were needed for illumination at the sample plane. Initially, an SLM was optically relayed directly onto the first scanning mirror using a pair of relay lenses (Fig. 1.4 (a)). Optically relaying allowed access to the image plane of the scan mirror, whilst the second relay controlled the magnification of pixel size of the SLM at the imaging plane of the excitation objective. The energy in each resultant beam, when a diffractive pattern was displayed on the SLM, was not equal due to the implementation being polarisation sensitive. This was compensated for by controlling the voltage of each pixel (which controlled the phase of the reflected photons) on the SLM but due to the discrete nature of the voltage being applied to each SLM pixel, the energies of each beam could not be sufficiently well matched. As well, due to the pixel nature of the SLM, the separation of the two beams (governed by the SLM pattern frequency) could only be discrete distances, with the step size being larger than a single pixel at the camera. Using an SLM also limited the potential for creating exotic illumination superimposed on the both beams. Though solutions do exist (using super-pixels[4], or dual SLMs[[fuImagingMulticellularSpecimens2016a](#)]) the methods are limited and heavily optically involved.

1.2.2 Dual slits using a fast galvanometric mirror

Conceivably, by driving the galvanometric mirrors at a very high frequency and pulsing a laser appropriately, a pulsed sampling of the laser could emulate two independent laser sources moving in unison. This solution would require no additional optics. To realise this, the round trip time of the scanning mirror, would in the best case, have to match the time it takes for the shutter to move up one row of pixels, $\frac{10\text{ ms}}{1024} = 9.8\text{ }\mu\text{s}$. Therefore, the drive frequency would then exceed 100 kHz, which is currently infeasible with most commercial scanning mirror technology and most affordable visible lasers.

1.2.3 An all optical dual-slit implementation

An alternative implementation was employed whereby, immediately follow the four spatially co-aligned colours, a beam splitter was added with two returning mirrors (similar to Michelson interferometer). The beam arms were not optically interfered,

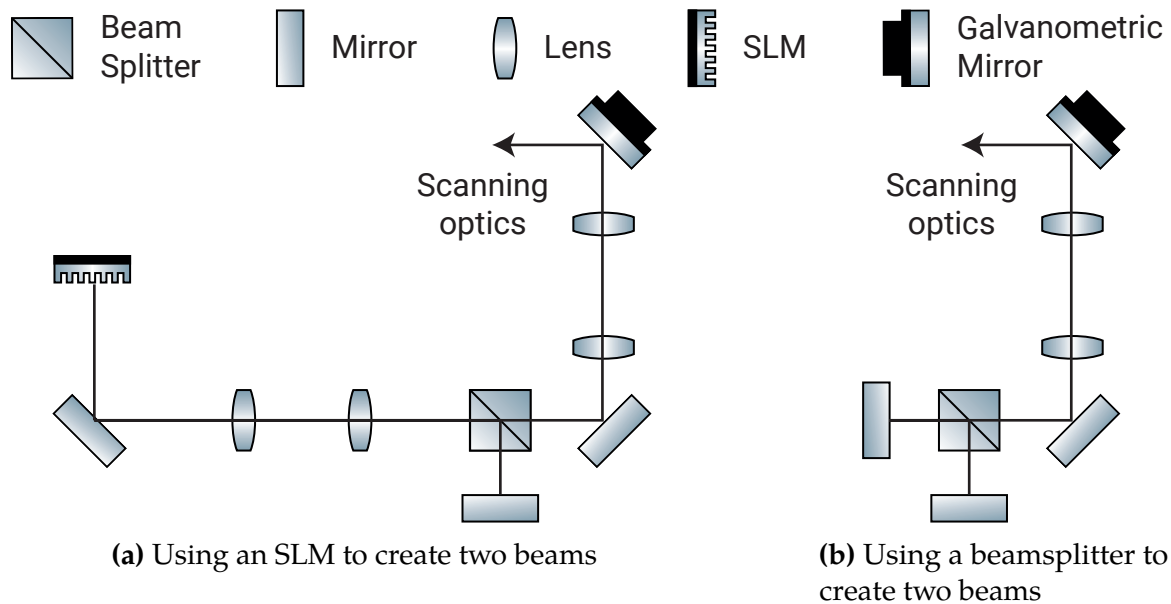


Fig. 1.4 Designs for possible optical layouts to create dual-beams in a DSLM system. (a) shows the conjugation of the SLM to the first scanning mirror, this technique suffered for optical losses on the SLM; discrete angular steps limited by the pixel size on the SLM and inhomogeneous distribution of power into each beam. (b) shows an optical solution for create two beams by using a beamsplitter.

instead they were purposely aimed-off to create a small angle in their propagation before reaching the scanning mirror (Fig. 1.4 (b)). This slight angular difference, once imaged through the telecentric scan lens, then became a spatial separation at the imaging plane of the system and was easily tuned using the kinematic mirrors flanking the beam splitter.

The all optical approach offered many key advantages: the system was polarisation insensitive and suffered minimal optical losses, especially when compared to using an SLM; as the duplication of the beams was now independent of any beam shaping, actual beam shaping optics could be readily implemented, this had the potential for optics such as cubic phase masks and axicon lenses or even an SLM being inserted to structure the beams.

Two laser beams were created at the image plane that could be manually separated as imaged in Fig. 1.5. To position the beams the correct distance apart, the bottom most beam was aligned to middle of the FOV by reducing the FOV of the camera by half digitally and aligning the *primary* beam with the bottom of the image using the galvanometric mirror. The *secondary* beam was pushed to the top of the image using an appropriate the kinematic mirror flanking the beam splitter.

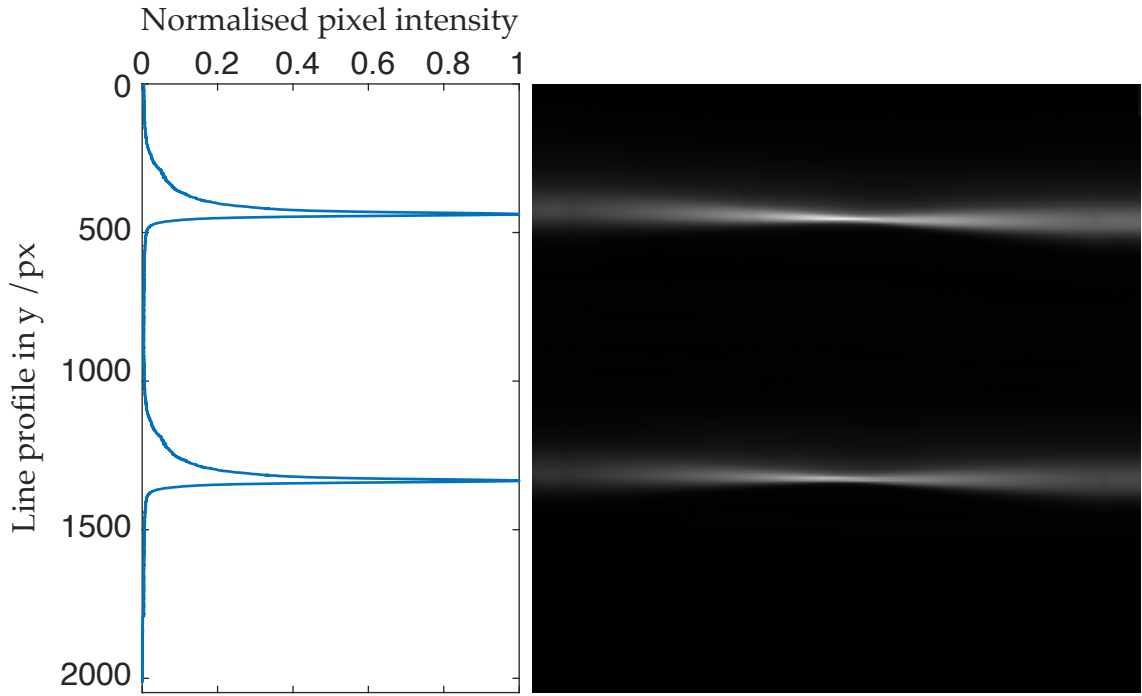


Fig. 1.5 Fluorescence image of two beams at image plane as profiled by a solution of Rhodamine.

1.3 Structured illumination enhanced with slit-scanning

1.3.1 Widefield

A similar effect to a swept beam in a light-sheet system can be realised in a wide-field system using an SLM. By conjugating an SLM to the image plane of the objective, with suitable polarisers, activate pixels on the SLM will exclusively illuminate the corresponding region in the image plane. To then mimic a scanning light-sheet, as above, a row of SLM pixels are activated and the line synchronously swept with the confocal virtual shutter on the camera. With this, the contrast and resolution of the output image increases in the direction of propagation of the shutter as simulated in Fig. 1.6 using the equation:

$$I_{\text{em}}(x, y, n) = \sum_{n=0}^{n=h-1} \left([(s(x, y) \cdot (I_{\text{ill}}(x, y, n) * \text{PSF}(x, y))) * \text{PSF}(x, y)] \right) \cdot H(y - n) \cdot H(-(y - n) + w_{\text{slit}}) \quad (1.2)$$

Where $0 \leq x < w$ and $H(y)$ is the Heaviside step function:

$$H(y) = \int_{-\infty}^y \delta(s)d(s) \quad (1.3)$$

The sample $s(x, y)$ is illuminated with a spatial pattern of $I_{\text{ill}}(x, y, n)$ (which may vary during an exposure, as in light-sheet microscopy) and imaged onto a detector with width w and height h . n is the pixel number of the active row as the shutter rolls; $H(y - n) \cdot H(-(y - n) + w_{\text{slit}})$ represents the active region on the detector as the shutter rolls with a width of w_{slit} and $\text{PSF}(x, y)$ is the point-spread function.

For flat wide-field illumination

$$I_{\text{ill}}(x, y, n) = I_0 \quad (1.4)$$

and for slit-scanning flat wide-field illumination

$$I_{\text{ill}}(x, y, n) = I_0 \cdot H(y - n) \cdot H(-(y - n) + w_{\text{slit}}) \quad (1.5)$$

For DSLM illumination

$$I_{\text{ill}}(x, y, n) = I_0 \left(\frac{w_0}{w(y + n)} \right)^2 e^{\frac{-2x}{w(y + n)^2}} \quad (1.6)$$

As the imaging and illumination objective lens are not the same, $I_{\text{em}}(x, y, n)$ is now

$$I_{\text{em}}(x, y, n) = \sum_{n=0}^{n=h-1} \left([(s(x, y) \cdot I_{\text{ill}}(x, y, n)) * \text{PSF}(x, y)] \cdot H(y - n) \cdot H(-(y - n) + w_{\text{slit}}) \right) \quad (1.7)$$

The application of confocal slit-scanning was also considered for structured illumination sources.

1.3.2 Slit-scanning Structured Illumination Microscopy (SIM)

In the case of SIM and multi-focal Structured Illumination Microscopy (mSIM), patterned light is projected onto a sample to provide a resolution doubling after a reconstruction step, as discussed in Chapter ???. SIM relies on frequency mixing to shift high resolution information from outside the pass band of the objective into the observable, reminiscent of a heterodyne.

High contrast fringes are needed so that sharp peaks can be localised from the sinusoidal illumination pattern. Fringe contrast in real-space corresponds to SNR of these peaks. An accurate SIM image can then be reconstructed once the (\mathbf{k}) vectors in frequency space are recovered. If the localisation of these points is inaccurate, computationally inverting the frequency mixing of the illumination and the sample will cause the final image to have artefacts. As discussed, slit-scanning has the potential to increase image contrast without sacrificing on speed of acquisition; to achieve this in SIM requires a fast ferroelectric SLM, with a refresh rate better than the imaging camera. For slit-scanning SIM as in slit-scanning wide-field, a row of active pixels is swept during an exposure but now this pattern is the product of a standard set of SIM patterns as shown in Fig. 1.7. For these simulations 9 unique patterns were used, 3 oriented patterns with each 3 phases; though fewer can be used[5]. Slit-scanned SIM simulations of a test image were successfully reconstructed, as seen in Fig. 1.8, with the spatial illumination as:

$$I_{\text{ill}}(x, y, n) = I_0[1 + \cos(k_x x + k_y y + \phi)] \cdot H(y - n) \cdot H(-(y - n) + w_{\text{slit}}) \quad (1.8)$$

At one of 3 angles $\theta = \frac{k_x}{k_y}$ and one of 3 phases (ϕ).

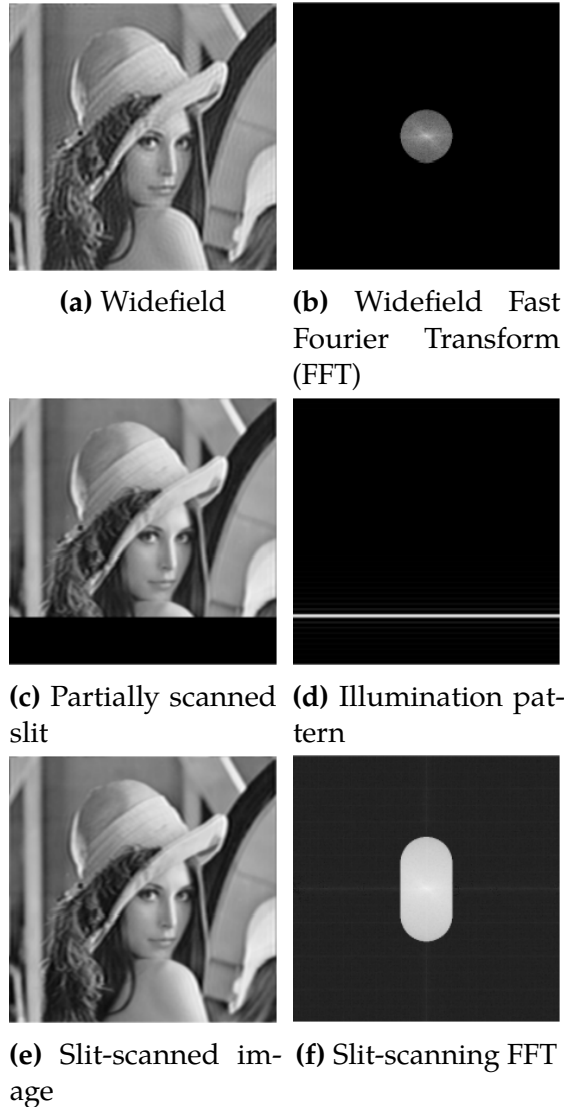


Fig. 1.6 Simulation of a confocal slit-scanned wide-field or swept light-sheet system. (a) is the raw, image with (b) showing Fourier space and the frequency passband. (c) Shows the confocal slit-scanning in progress and (d) shows what the SLM will be displaying. (d) is the final image as it would appear after an acquisition and (e) is the new Optical Transfer Function (OTF) with a larger support in y .

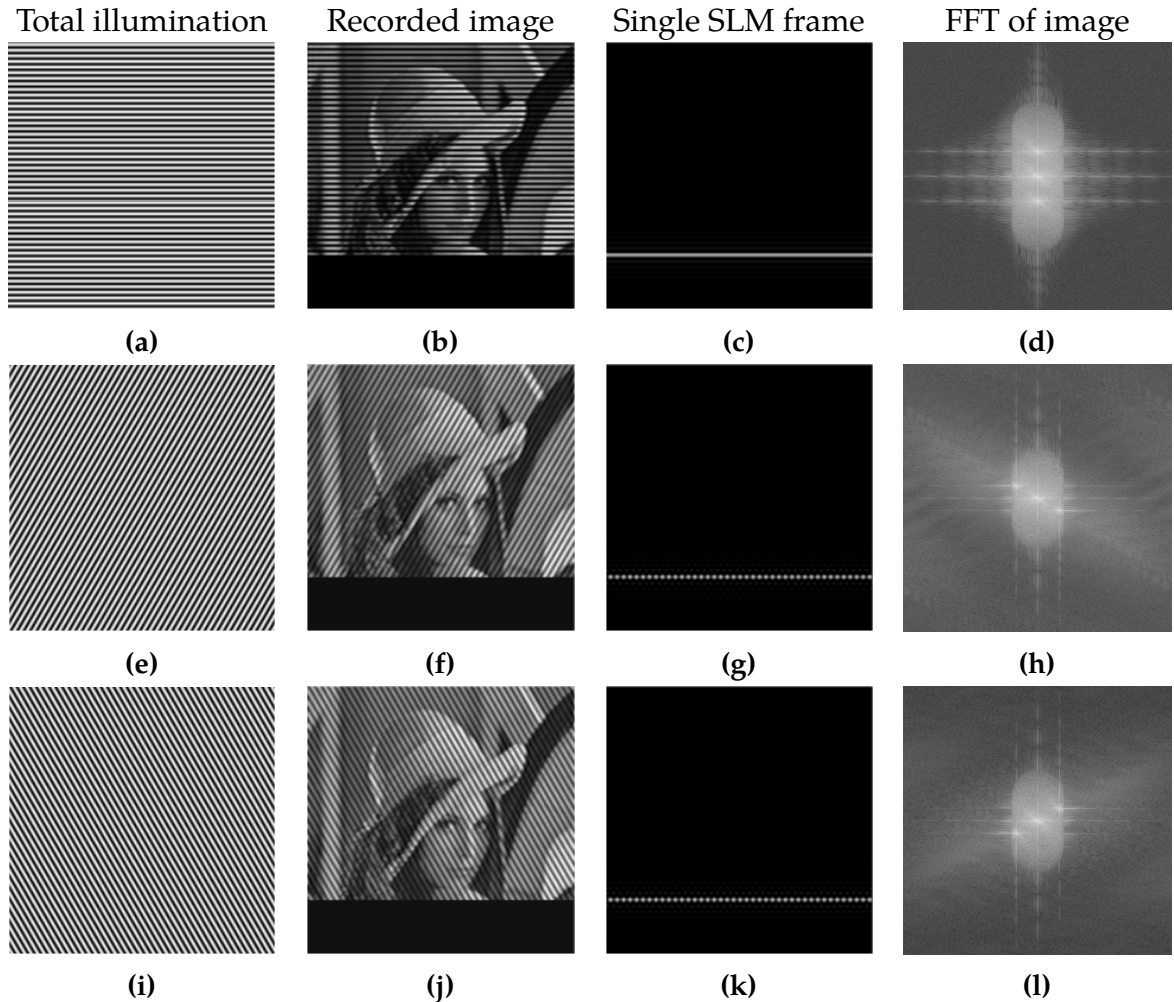


Fig. 1.7 (a),(e) and (i) are the three SIM angles traditionally used for reconstruction. (b),(f) and (j) are these illuminations during a partial single frame exposure and (c),(g) and (k) are the respective patterns as displayed on an SLM; giving the final images (d),(h) and (l) as seen in frequency space with the larger OTF support.

1.3.3 Slit-scanning mSIM

The same principle for slit-scanning SIM can be also be applied to mSIM. mSIM uses a square lattice of points, raster scanned across the sample to provide a fast, parallelised, confocal-like image. Each spot is computationally pin-holed, and the resulting images are summated to produce a final, super-resolved image.

In slit-scanning mSIM, during each exposure, the SLM will display a single row of illumination spots from the full lattice with a standard mSIM pattern. This row is then swept synchronously with the virtual slit as with slit-SIM. For the proceeding

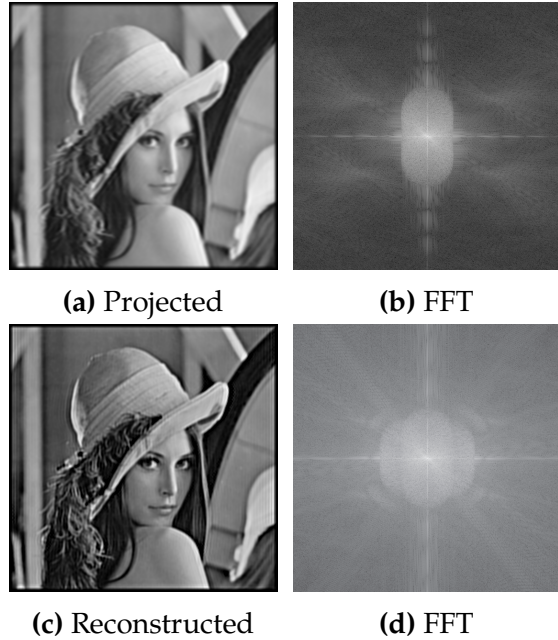


Fig. 1.8 slit-SIM images as reconstructed using fairSIM. (a) The projected sum of the 9 raw SIM images with (b), the complimentary Fourier space image which shows the diffraction limited information along the horizontal. (c) The slit-SIM reconstruction with (d), the Fourier space image showing the OTF support being extended along the horizontal.

exposure, the line of point illuminators is iterated in the orthogonal direction to the propagating shutter.

The act of using a virtual slit on the camera reduces the dimensionality of the reconstruction of an mSIM image, drastically increasing the speed of an acquisition without the need for additional optics. Ordinarily, the virtual pin-holing step is achieved computational by reconstructing from an $n \times n$ ($O(n^2)$) set of images; using slit-scanning the reconstruction reduces to n ($O(n)$) operations. Schroff *et al.*, for instance, require 200×200 images for a single mSIM reconstruction. The method proposed here, would potentially increase the speed of this process by 200 fold. This is however dwarfed by instant Structured Illumination Microscopy (iSIM), which gives instantaneous super-resolved images at the cost of requiring extensive additional optics[6]. Through computer simulation it was shown, in Fig. 1.9, that the OTF support of the reconstructed mSIM image increases in one direction up to 2 fold in ideal conditions and a slit width (w_{slit}) of one pixel. Using fewer images can reduce the amount of acquisition time needed, but as slit-scanning does reject photons there may be a trade-off in real samples when acquiring a sufficient number of photons to reconstruct an image, potentially increasing exposure times.

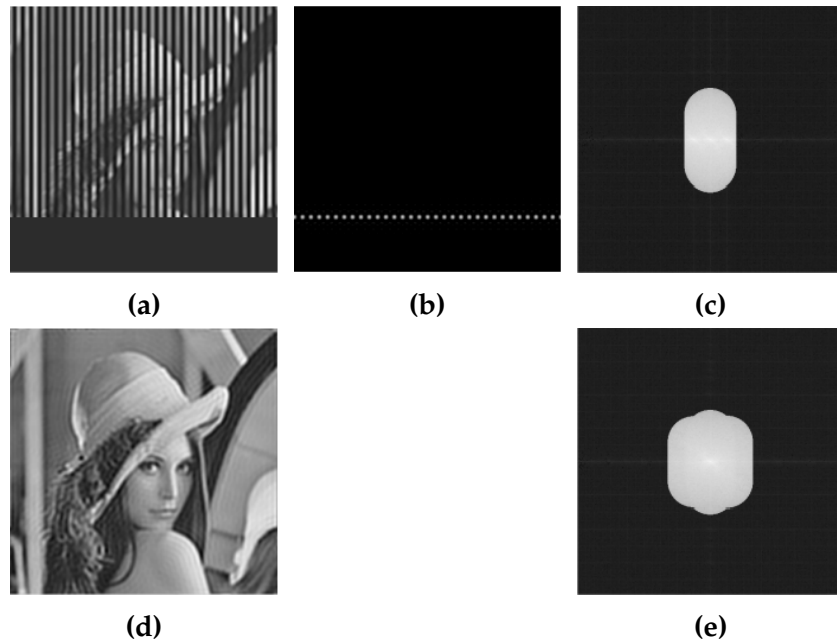


Fig. 1.9 (a): The capturing of a single mSIM frame; (b): mSIM illumination pattern as it rolls; (c): The OTF of a single mSIM frame; (d): The reconstructed slit-mSIM image; (e): The FFT of a reconstructed slit-mSIM frame, now with a wider OTF support.

1.4 Discussion and future work

1.4.1 Dual slit-scanning

Confocal slit-scanning can now be achieved at full 100 Hz imaging rates and so could be applied to fast dynamic processes in need of contrast and axial resolution improvements. The intent with this work was to apply the improvement provided by slit-scanning to Single Particle Tracking (SPT), as time resolution is essential for characterising motion; similarly a large field of FOV would mean particles can be tracked for longer times periods of time. In having two independently addressable sensors another technique which can be implemented is chromatically separating the two channels on to each of the sensors, providing simultaneous two colour 100 Hz imaging. Such image splitting devices are commercially available[7], with the trade-off of FOV for time-resolution. Due to the additional optics added to the light-sheet system for the astigmatic tracking module, there was not sufficient space to investigate this technique further.

1.4.2 Structured illumination slit-scanning

The effect of confocal slit-scanning was explored *in silico*, to verify the expectation that resolution and contrast could be improved using confocal slit-scanning. This was considered for systems imaging orthogonally, such as is light-sheet microscopy, as well for epi-illumination systems with control over the the illumination structure.

The techniques simulations presented here can be immediately adapted onto microscope systems with SLMs already embedded, provided there is intensity (rather then phase) control at the sample plane. For a $512\text{ px} \times 512\text{ px}$ FOV, at 40 ms exposure, the SLM would need to be run at 12.8 kHz which is only viable for ferroelectric liquid crystal SLMs.

Reconstructions for SIM were achieved using fairSIM, an open-source SIM reconstruction package implemented in Java for ImageJ[[mullerOpensourceImageReconstruction2016a](#)]. However, fairSIM assumes that each angle provided will have the same size OTF at each illumination angle. When using slit-scanning the OTF support becomes larger in the direction of the rolling shutter; as such fairSIM, though it reconstructs successfully, omits additional resolution in one direction. To realise slit-scanning SIM, a custom reconstruction algorithm will be needed to maximally fill the reconstructed frequency space, by using asymmetric OTFs.

It was expected that the contrast improvement in SIM would be the primary benefit to the technique. However, it may be possible exploit the increase in resolution in one direction to increase the resolution of SIM further. Currently fairSIM only considers possible OTF supports which have rotational symmetry. The addition of confocal slit-scanning means that, though the reconstruction is successful, higher resolution information afforded by slit-scanning, is neglected. Going further, it may be possible in a real system to display a very fine SIM pattern in the direction of confocal slit-scanning. The Moir  fringes of this image would ordinarily be blurred to the point where the SIM pattern in Fourier space would be outside of the passband. Using slit-scanning with SIM may allow the recovery of these fringes, for reconstruction, potentially giving up to a $4\times$ resolution improvement, with better optical sectioning and contrast.

References

1. Sabharwal, Y. S., Rouse, A. R., Donaldson, L., Hopkins, M. F. & Gmitro, A. F. Slit-Scanning Confocal Microendoscope for High-Resolution in Vivo Imaging. *Applied Optics* **38**, 7133–7144 (1999).
2. Baumgart, E. & Kubitscheck, U. Scanned Light Sheet Microscopy with Confocal Slit Detection. *Optics express* **20**, 21805–14 (2012).
3. Jahr, W., Schmid, B., Schmied, C., Fahrbach, F. O. & Huisken, J. Hyperspectral Light Sheet Microscopy. *Nature Communications* **6**, 7990 (2015).
4. Van Putten, E. G., Vellekoop, I. M. & Mosk, A. P. Spatial Amplitude and Phase Modulation Using Commercial Twisted Nematic LCDs. *Applied Optics* **47**, 2076–2081 (2008).
5. Ströhl, F. & Kaminski, C. F. Speed Limits of Structured Illumination Microscopy. *Optics Letters* **42**, 2511–2514 (2017).
6. York, A. G. *et al.* Instant Super-Resolution Imaging in Live Cells and Embryos via Analog Image Processing. *Nature Methods* **10**, 1122–1126 (2013).
7. *Emission Image Splitter | OptoSplit II Image Splitter | Cairn Research Ltd* <https://www.cairn-research.co.uk/product/optosplit-ii/> (2018).